Nanoscale

Accepted Manuscript

Cite this: DOI: 10.1039/c0xx00000x

www.rsc.org/xxxxxx

ARTICLE TYPE

Targeted delivery of photosensitizers: efficacy and selectivity issues revelead by multifunctional ORMOSIL nanovectors in cellular systems.

Francesco Selvestrel,[a,‡] Francesca Moret,[b,‡] Daniela Segat,[c,‡] Josephine H. Woodhams,[d‡] Giulio Fracasso,[e,‡] Iria. Rio Echevarria,[a] Luca Baù,[a] Federico Rastrelli,[a] Chiara Compagnin,[b] Elena Reddi,*[,b] Chiara Fedeli,[c] Emanuele Papini,[c] Regina Tavano,*[,c] Alexandra Mackenzie,[d] Melissa Bovis,[d] Elnaz Yaghini,[d] Alexander J. MacRobert,*[,d] Silvia Zanini,[e] Anita Boscaini,[e] Marco Colombatti,*[,e] and Fabrzio Mancin*[,a]

Received (in XXX, XXX) Xth XXXXXXXXX 20XX, Accepted Xth XXXXXXXXX 20XX
DOI: 10.1039/b000000x

PEGylated and non-PEGylated ORMOSIL nanoparticles prepared by microemulsion condensation of vinyltriethoxy-silane (VTES) were investigated in detail for their micro-structure and ability to deliver photoactive agents. With respect to pure silica nanoparticles, organic modification substantially changes the microstructure and the surface properties. This in turn leads to a modulation of both the photophysical properties of embedded photosensitizers and the interaction of the nanoparticles with biological entities as serum proteins. The flexibility of the synthetic procedure allows the rapid preparation and screening of multifunctional nanosystems for photodynamic (PDT) therapy. Selective targeting of model cancer cells was tested by using folate, integrin specific RGD peptide and anti-EGFR antibodies. Data suggest the interference of the stealth-conferring layer (PEG) with small targeting agents, but not with bulky antibodies. Moreover, we showed that selective photokilling of tumour cells may be limited even in the case of efficient targeting because of intrinsic transport limitations of active cellular uptake mechanisms or suboptimum localization.

Introduction

Over the last few years, silica nanoparticles have attracted a great deal of interest as materials for biomedical applications.[1] At first glance, this may appear quite surprising. Unlike other nanomaterials, silica nanoparticles do not have any nanosize-related properties, nor are they easily biodegraded.[2] So, what makes silica nanoparticles so attractive? The answer lies in their highly cross-linked polymeric nature. Being of polymeric structure they can accommodate in their interior (either in the silica matrix or within pores) active molecules, such as drugs, dyes and photosensitizers.[3] The loading capacity of silica nanoparticles is hence much higher than that achievable with other nanomaterials which allow only surface grafting, and this enables their use for drug delivery applications. On the other hand, their highly cross-linked nature renders silica nanoparticles much more rigid than other polymeric nanoparticles. This makes it possible to process them into very complex structures, including mesoporous particles,[1c,4] nanoshells[5] and multi-shell particles.[3,6] Such versatility has opened the way to the realization of several sophisticated systems, such as gated porous particles for controlled release,[1a,f] multimodal imaging and delivery agents,[1] chemical sensors.[7] Notably, silica does not need to be made only by silicon oxide. Using organosilane precursors in the formation of the silica network, organically modified silica (ORMOSIL) materials can be obtained.[8] Here, the possibilities for tuning the nanoparticles properties, either of the surface and

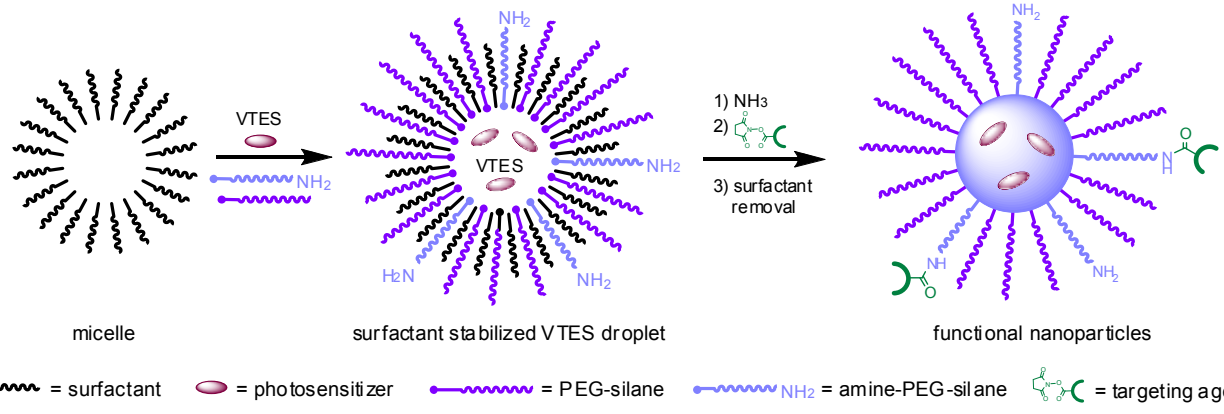

Scheme 1. One-pot synthesis of doped, PEGylated and functional ORMOSIL nanoparticles. Any of the components indicated in the caption, with the exception of the surfactant may be omitted to prepare nanoparticles with different features.

Cite this: DOI: 10.1039/c0xx00000x

www.rsc.org/xxxxxx

ARTICLE TYPE

of the bulk phase, or by changing the nature of the organic moiety introduced, are very broad. A class of ORMOSIL nanoparticles that has recently emerged as an attractive candidate for nanomedicine applications comprises those prepared by the base-catalyzed condensation of vinyl-triethoxysilane (VTES, chart 1) in aqueous surfactant solutions.

This synthetic protocol was first proposed by P. N. Prasad and co-workers in 2003 for the development of photosensitizer delivery agents in photodynamic therapy (PDT).[9] This approach enabled a series of very elegant advances stemming from the original photosensitizer loaded particles,[10] including two-photon excitation of the photosensitizer through Förster energy transfer from a co-included antenna[11] and matrix enhancement of the singlet oxygen production quantum yield.[12] Applications for fluorescent probes,[13] encapsulation of other nanoparticles,[14] DNA transfection[15] and targeted delivery[16] were also reported.

Advantages of such ORMOSIL nanoparticles are many. Firstly, the use of the organosilane precursor provides a low polarity interior that favours the inclusion of hydrophobic molecules but does not prevent their release in biological fluids.[17] Secondly, the properties of both the bulk material and probably also of the particles surface may be tailored, as mentioned earlier, by the use of different organosilane precursors. But the most relevant feature is brought about by the microemulsion polymerization protocol used for their preparation. In fact, not only does the surfactant aggregate act as a nanocontainer where the organosilane polymerization is confined, but it can also play the role of a template, where it pre-organizes the nanoparticle components placing them precisely in the site they are needed to perform their function. Hence, as demonstrated by Prasad and also by us, dye-doped surface functionalized nanoparticles can be prepared by a one pot-procedure.[16,18] Indeed, we recently showed, by taking full advantage of such an approach, that densely PEGylated nanoparticles can be prepared[18] and that such a dense coating reduces the toxic[19] and pro-coagulant[20] properties of particles themselves and avoids capture by immune system cells.[18] While these findings further amplify the interest in nanomedicine applications of ORMOSIL nanoparticles, their structure and characteristics have yet to be fully investigated. By a detailed investigation of the chemical, structural and biological properties of PEGylated and non-PEGylated ORMOSIL nanoparticles made with VTES, we have acquired herein a deeper comprehension of their properties and potential for applications.

Results and Discussion

Chemical microstructure and surface properties

The synthesis of the VTES-ORMOSIL nanoparticles (Scheme 1) may be regarded as a variation of the well-known Stober procedure,[21] involving the ammonia-catalysed polymerization of alkoxysilane precursors in ethanol. The main difference here is that the reactions occur in water and in the presence of a surfactant (AOT, Tween, Brij) that controls the growth of the

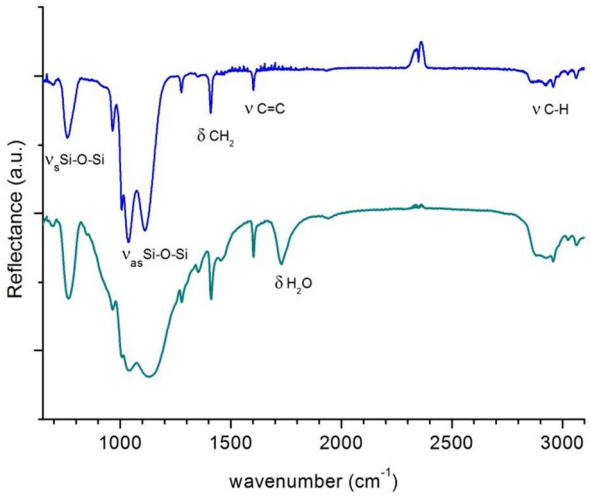

Figure 1. ATR-IR Spectra of lyophilized ORMOSIL nanoparticles (blue) and PEGylated ORMOSIL nanoparticles (green).

nanoparticles. Such modifications and the use of an organosilane precursor may influence the nanoparticles microscopic structure. With this view, we prepared VTES nanoparticles with a diameter of 50 nm using the Brij surfactant for spectroscopic characterization. The ATR-IR spectrum (Figure 1, blue) contains all the main features of VTES-containing materials.[22] The most intensive band, at about 1100 cm^{-1} is due to the asymmetric stretching of the Si–O–Si bridges, and, as usually found for ORMOSIL materials, splits into two separate bands at 1040 (TO mode) and 1110 (LO mode) cm^{-1}. Interestingly, the position of these signals is 20-40 nm red-shifted with respect to the usual values found in VTES containing sol-gel films prepared by acid catalysis,[22] possibly indicating a highly porous structure of the nanoparticles. The symmetric stretching of the same silicon–oxygen bridges is responsible of the band at about 760 cm^{-1}. The sharp signals at 1409 (in plane CH_2 bending) and 1602 (C=C stretching) cm^{-1} arise from the vibrations of the vinyl groups. On the other hand, the sharp signal at 966 cm^{-1}, is likely the result of the overlap of the signals arising from Si-OH stretching and vinyl CH_2 wagging.

More detailed structural information is obtained by MAS solid state NMR. ^{13}C NMR (Figure 2a, blue) confirmed the complete hydrolysis of the alkoxysilane precursor since no signals related to the ethoxy moieties are visible in the spectrum. The two-broad signals at 145 and 135 ppm arise from the two carbon atoms of the vinyl residues. On the other hand, a series of sharp signals is visible between 80 and 20 ppm, which corresponds very well to the Brij surfactant. We were not able to remove the surfactant signals either by extensive ultrafiltration or Soxlet extraction with boiling ethanol, indicating that it is likely physically entrapped in the ORMOSIL matrix. The ^{29}Si spectrum (Figure 2b, blue) shows two signals at -77 and -68 ppm, arising respectively from fully condensed T^3 and partially condensed T^2 silicon atoms.

Integration of the signals indicates that T^2 atoms are only 10% of

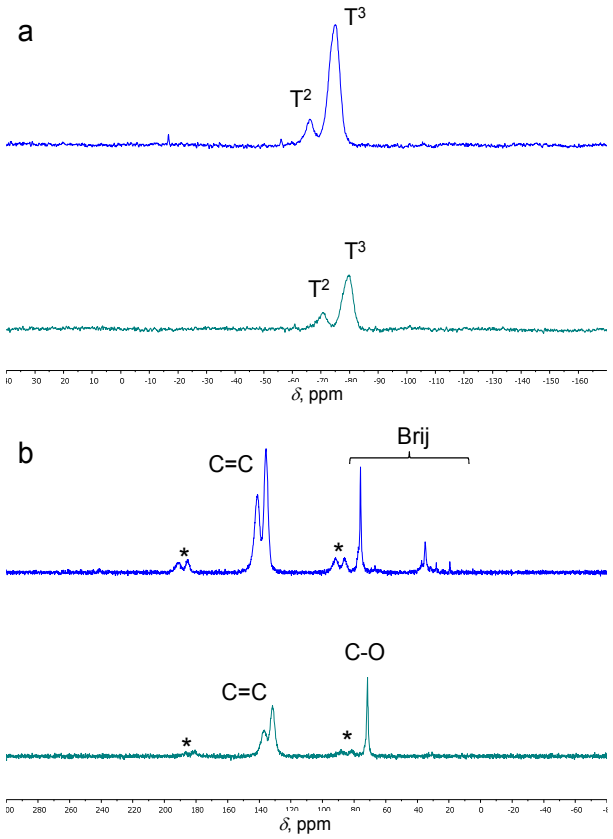

Figure 2. ^{29}Si MAS (a) and ^{13}C MAS (b) solid state NMR of lyophilized ORMOSIL nanoparticles (blue) and PEGylated ORMOSIL nanoparticles (green). C=C indicates the vinylic carbons and C-O the carbons bound to oxygen of the PEG polymer. The symmetric signals (*) at 70 and 170 ppm in the ^{29}Si spectrum are spinning bands.

the total, indicating a highly condensed structure. When compared with pure silica nanoparticles, the VTES ORMOSIL particles reveal interesting differences. Early studies by van Blaaderen indicated that silica nanoparticles prepared either via the Stöber protocol (TEOS condensation in ethanol) or via the micro-emulsion protocol (TEOS condensation in water/ cyclohexane microemulsion) are characterized by incomplete hydrolysis of the precursor alkoxysilanes and much less condensed structure (67 and 55% of fully condensed Q^4 silicon atoms, respectively).[23] Only the commercial Ludox particles, that are prepared by condensation of silicates in water, present a similarly highly condensed structure, with 85% of Q^4 silicon atoms.[23]

The degree of hydrolysis and condensation, however, does not influence surface charge, which is one of the most important features of nanoparticles for biomedical applications since it determines their stability in high ionic strength biological fluids and ability to interact with cells. Z-potential measurements performed in PBS buffer at pH 7.4 yielded he values of -5.9, -18.3 and -15.6 mV respectively for ORMOSIL, Stober and Ludox particles (50 nm diameter). Hence, surface charge is not proportional to the amount of acidic Si-OH groups present on the particles (corresponding to partially condensed silicon atoms), which is greater in Stober particles and smaller in ORMOSIL and Ludox. Van Blaaderen calculations reveal that surface silanols

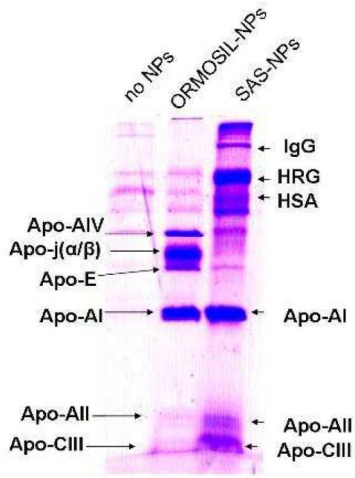

Figure 3. Comassie Blue stained SDS-PAGE analysis of nanoparticle-bound human plasma proteins.

account for a very small fraction (2,5% for 50 nm diameter nanoparticles) of the total silicon atoms.[23] Hence, even in the most condensed particles the amount of silanols detected by ^{29}Si MAS NMR groups largely exceed that necessary for a full surface coverage. This explains why Stober and Ludox particles have similar Z-potential values notwithstanding the large difference in number of silanols. Once all the available sites on the surface are occupied, silanols in excess must locate in the nanoparticles interior not affecting the overall surface charge. Hence, in the case of ORMOSIL particles, the less-negative Z-potential could be explained by postulating that several vinyl moieties are exposed on surface instead of OH groups, and this reduces the overall surface charge. The consequences of such a relevant difference in the surface chemical structure should be observed not only on the Z-potential values but also on the interaction with serum proteins, which is fundamental in determining the biological fate of the nanoparticles.[24] To test this hypothesis the patterns of protein adsorbed on ORMOSIL and Ludox particles, after 3 hours incubation at 37°C in human plasma, were identified by SDS-PAGE and mass spectroscopy (figure 3). Interestingly, both ORMOSIL and Ludox particles recruit few and quite different plasma proteins, with Ludox interacting preferentially with Immunoglobuline-G (IgG), Histidine Rich Glycoprotein (HRG), Human Serum Albumin (HSA) and apolipoproteins ApoA-I, ApoA-II, and ApoC-III, while ORMOSIL exhibit higher affinity for ApoA-IV, ApoE, ApoJ and ApoA-I. Hence, the reduction of the surface charge (which still remains negative) and the exposure of vinyl residues results in a shift of preference from soluble IgG, HSA and HRG proteins to more hydrophobic lipoproteins. We previously observed that hydrophobic photosensitizers entrapped in the ORMOSIL where rapidly released from the nanoparticles when incubated with serum.[17b] The high preference for recruiting lipoproteins, which are known carriers of hydrophobic species, could account for this observation.

As we have shown earlier, addition of an amphiphilic trialkoxysilane PEG derivative to the reaction mixture, as **1** in Chart 1, results in the formation of densely PEGylated nanoparticles.[18] PEGylation produces only minor modifications on the IR spectrum (Figure 1, green) where a broadening of the

Cite this: DOI: 10.1039/c0xx00000x
www.rsc.org/xxxxxx

ARTICLE TYPE

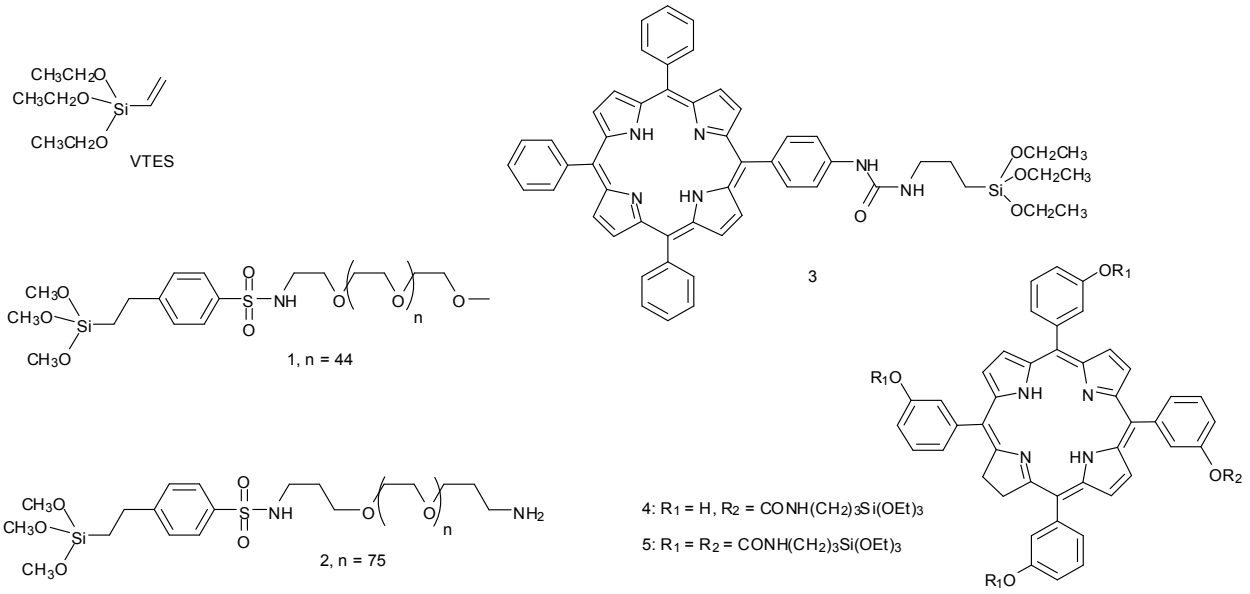

Chart 1. Alkoxysilane derivatives used in this work

signals in the 1000-1200 cm^{-1} range, due to the superimposition of the PEG signals, is the main difference observed. PEG features are also visible in the ^{13}C MAS solid state NMR signal at 71 ppm, arising from the methylenes of the polyethylene oxide chain (Figure 2b, green). Analysis of this spectrum also reveals the absence of residual surfactant in these samples, in contrast with the non-PEGylated ORMOSIL nanoparticles (Figure 2b, blue). This suggests that the presence of the amphiphilic silane prevents the surfactant from remaining physically entrapped in the ORMOSIL matrix, hence favouring its removal. TGA analysis (ESI) reveals that the dense coat of PEG-2000 accounts respectively for 67, 38 and 25% of NPs weight for nanoparticles with 20, 55 and 70 nm diameters. Such figures lead to estimate a surface density of 1-2 PEG molecules per nm^2.

Finally, ^{29}Si-NMR indicates a smaller degree of condensation of the silicon atoms, with the amount of partially condensed T^2 atoms raised here to 34%. However, both the surface coating with PEG and again the presence of a larger amount of silanol groups in the ORMOSIL matrix appear not to affect the overall surface charge, the Z-potential (in PBS buffer, pH 7.4) being −4.3 mV, only slightly different form that of the "naked" ORMOSIL particles.

Photochemical properties of embedded photosensitizers

Having such a strong influence on the surface properties of the nanoparticles, the presence of the vinyl groups is expected to affect also the interior silica matrix and as a consequence the properties of embedded dyes. This aspect is particularly relevant for one of the most promising application of VTES-ORMOSIL nanoparticles, namely the anticancer modality called photodynamic therapy (PDT).[9-17] In this approach, a photosensitizing molecule should be selectively delivered inside the tumour and produce, upon activation with light, cytotoxic reactive oxygen species (ROS) that kill the tumour cells. Remarkably, the photosensitizer does not need to be released from the carrier to exert its phototoxic effect and therefore it can be embedded in the nanoparticles without the need of devising effective release mechanisms. However, the essential requirement is that the embedded photosensitizer maintains its photophysical properties and hence its ability to generate ROS, in particular singlet oxygen.

To investigate this point, we initially prepared both Stöber silica nanoparticles and VTES-ORMOSIL nanoparticles (both PEGylated and not) doped with the alkoxysilane porphyrin derivative **3** (we selected this molecule because most of the photosensitizers used in clinic are porphyrins or chlorins) and investigated the photophysical properties of the embedded dye. Inspection of the fluorescence lifetime data reported in Table 1 reveals that all the nanoparticles-embedded dyes (Entries 2-4) show biexponential decays with a long component (~10 ns) that is very similar to the life-time of **3** in ethanol (Entry 1) and a short component (~3 ns) which presumably arises from poorly emissive porphyrin aggregates. However, while the short component is minor in the ORMOSIL particles, it is predominant in the Stöber particles (Entry 2), where this behaviour is accompanied by a broadening of the porphyrin Soret band in the UV-Vis spectrum (ESI). This suggests that the more polar environment provided by silica matrix with respect to that of ORMOSIL favours the formation of weakly fluorescent dye aggregates inside the particles, which are known to be ineffective as photosensitizers.[25] Fluorescence self-quenching through interaction of adjacent photosensitiser moieties results in lower

Table 1. Photophysical properties (fluorescence lifetimes (τ) and their amplitudes (A), and singlet oxygen quantum yields (ϕ_Δ) of photosensitizers embedded in silica (Stöber) and ORMOSIL (OS) nanoparticles.[a,b]

Entry	Dye	Np	Solvent	τ_1/ns (A_1)	τ_2/ns (A_2)	ϕ_Δ[e]
1	**3**	-	EtOH	9.5 (100)		-
2	**3**	Stober[c]	H_2O	9.6 (55)	2.3 (45)	-
3	**3**	OS[c]	H_2O	11.2 (91)	3.0 (9)	-
4	**3**	OS/PEG[c]	H_2O	12.1 (85)	4.7 (15)	-
5	mTHPC	-	MeOH	8.4 (100)	-	0.71
6	**4**	-	MeOH	8.4 (100)	-	0.67
7	**4**	OS/PEG[d]	MeOH	8.5 (91)	0.8 (9)	-
8	**4**	OS/PEG	MeOH	8.6 (94)	1.0 (6)	0.55
9	**4**	OS/PEG	MeOH/H_2O	9.7 (90)	1.7 (10)	-
10	**4**	OS/PEG	H_2O	9.9 (83)	0.8 (17)	0.53
11	**5**	-	MeOH	8.3 (100)	-	0.65
12	**5**	OS/PEG[d]	MeOH	8.7 (78)	3.4 (22)	0.55
13	**5**	OS/PEG	MeOH	8.4 (88)	1.2 (12)	0.58
14	**5**	OS/PEG	MeOH/H_2O	9.9 (52)	0.8 (48)	-
15	**5**	OS/PEG	H_2O	10.0 (18)	0.7 (82)	0.10

[a] Nanoparticles diameter 20 nm and average photosensitizer loading 1.5% w/w unless otherwise stated. [b]Errors within 5%. [c]0.3% w/w photosensitizer loading. [d] 90 nm diameter. [e] ϕ_Δ measured in MeOD except Entries 10 and 15, which were carried out in D_2O

triplet state and singlet oxygen yields, and this interaction should therefore be minimised as far as possible. The less polar environment provided by the ORMOSIL matrix hence appears to be ideal for accommodating photosensitizer molecules with retention of their optimal photophysical properties.

More insight on this respect was obtained by studying the photochemistry of ORMOSIL nanoparticles containing the alkoxysilane derivatives **4** and **5** of the commercial photosensitizer mTHPC (Chart 1). Likewise in the previous case fluorescence decay profiles are biexponential, with the long component (~8-9 ns) similar to that of the free dye in methanol and a short component (~0.5-1 ns). mTHPC in MeOD ("monomeric mTHPC") exhibited a ϕ_Δ of 0.71, which is in agreement with the literature.[26]

In methanol, either mono- and tetra-functionalization of the parent mTHPC does not significantly alter the photophysical properties of the derivatives (Entries 5, 6 and 11). The singlet oxygen yields measured for mTHPC in MeOD are in good agreement with other studies.[26] Also embedding in the ORMOSIL matrix does not alter the photosensitizer properties (Entries 7-8, 12-13). In fact, in all these cases very similar emission lifetimes are observed with a major long-lived component and a minor short component. However, the situation drastically changes when moving to solvents with higher polarity (1:1 methanol/H_2O, H_2O). In the particles doped with **4** the long component remains predominant with only a slight increase of the short-lived one in more polar solvents (Entries 8-10). However, in the particles doped with **5,** the amplitude of the short component is substantially increased in water so that it becomes the dominant decay component. The fluorescence emission intensity is also substantially quenched compared to methanol (Entries 13-15). The behaviour of the emission quantum yield parallels that of the singlet oxygen quantum yield (measured by singlet oxygen phosphorescence at 1270 nm). Singlet oxygen production of nanoparticles doped by both the dye in methanol and by dye **4** in deuterated water are very similar to that of mTHPC in deuterated methanol, on the other hand, singlet oxygen production by **5**-doped nanoparticles in deuterated water is much lower (Entry 15).

The peculiar behaviour of the embedded dye **5** is not due to aggregation since it is not loading-dependent (not shown). In this case we propose that the penetration of water and resulting H-bonding inside the nanoparticle may lead to distortion of the tetra-coordinated chlorin macrocycle since it is rigidly attached to the silica matrix and cannot compensate by conformational realignment, unlike the mono-coordinated chlorin which is able to rotate. Distortion in the macrocycle planarity is well known to increase the rate of internal conversion resulting in quenching of its emission and singlet oxygen production.[27]

Targeting of the ORMOSIL nanoparticles

As we earlier demonstrated, functional groups for conjugation of the nanoparticles to targeting species can be introduced in the coating layer by simply adding a second PEG-trialcoxysilane derivative bearing a reactive terminal group (Scheme 1).[18] To further explore such possibility we prepared several batches of **4**-doped ORMOSIL nanoparticles targeted with different bioactive molecules, such as folic acid, biotin, the cyclic (RGD) peptide and the antibody Cetuximab (Chart 2). The nanoparticles were prepared in different sizes (20-100 nm) by adding to the reaction mixture different amounts of PEG derivatives **1** and **2** (1-30%). In the case of folic acid and biotin, which can be directly linked to the nanoparticles amino groups via the formation of an amide bond, targeting was performed by directly adding O-hydroxysuccinimmide ester derivatives of the targeting agents to the reaction mixture before the purification (Scheme 1). In this way, dye-doped, PEGylated and targeted nanoparticles could be prepared by a simple one-pot procedure. The grafting of folate and biotin to the nanoparticles was demonstrated by the presence of the characteristic spectral features of this molecule in the UV-Vis spectrum in the case of the first, and by the HABA-Avidin and the EZview Red Streptavidin Affinity Gel tests for the second (see ESI).

On the contrary, the cyclic(RGD) peptide, which targets the $\alpha_v\beta_3$ integrin associated to tumor neovasculature (Chart 2), and the Cetuximab antibody, recognizing the Epithelial Growth Factor receptor (EGFR) overexpressed in many tumours, were conveniently conjugated to the nanoparticles by taking advantage of thiols group inserted in the derivatives (i.e. in the case of Cetuximab thiols group were introduced by reaction with 2-iminothiolane). This required the conversion of the terminal amine groups of the nanoparticles into thiol-reactive maleimide groups via the reaction with the commercial MBS crosslinker (Chart 2). Subsequent reactions with the cyclic(RGD), the inactive analogue cyclic(RAD) and iminothiolane modified Cetuximab antibody provided the targeted nanoparticles. In this case, due to the sensitivity of the maleimide group to nucleophiles, and to prevent unwanted conjugation between the targeting peptide and unreacted MBS, we preferred to perform the conjugation with a three step procedure involving

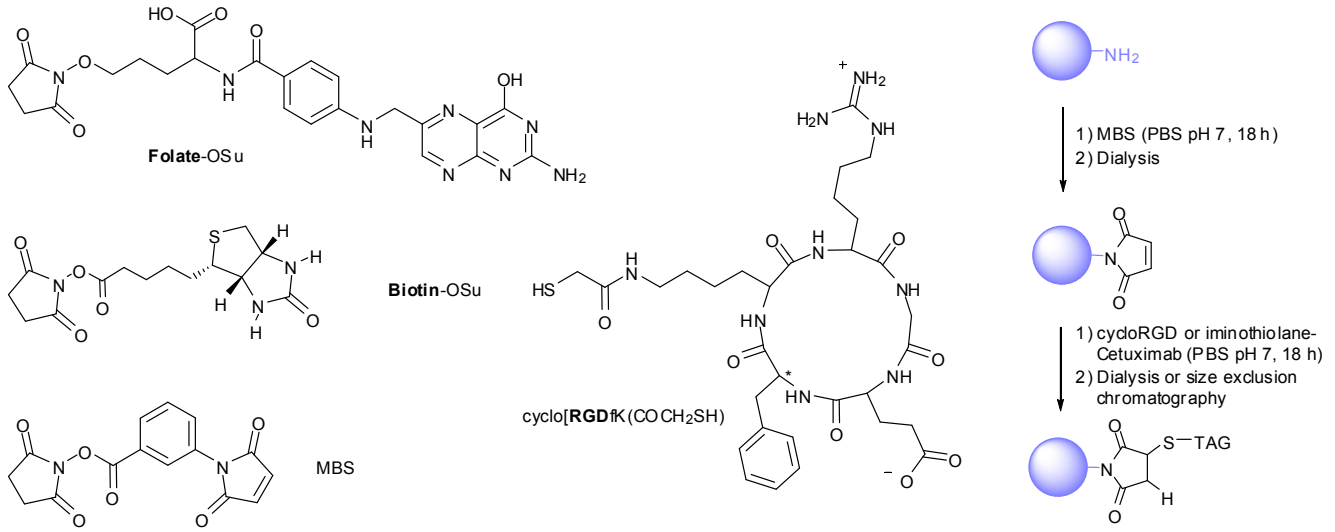

Chart 2. Targeting agents used and scheme for the post-synthetic functionalization of **1**/**2**-coated nanoparticles with the peptides and antibodies (TAG).

nanoparticles purification after each step (Chart 2). Antibody conjugation was confirmed by Western Blot analysis (see ESI).

Cellular uptake and targeting

In order to investigate the ability of the PEGylated ORMOSIL nanoparticles to enter cancer and healthy cells, free mTHPC and **4**-doped nanoparticles (90 nm diameter) were incubated, at the same dye concentration, with human lung carcinoma cells A549 and normal lung fibroblasts CCD-34Lu for 24 h at 37 °C in culture medium supplemented with 3% fetal calf serum (FCS). The dye uptake was measured by flow cytometry (FACS) experiments using the fluorescence emission of the chlorins associated to the cells. As expected, the cellular uptake of the drug by both the cancer (Figure 4) and healthy cells (ESI, Figure S10) is greatly reduced by the embedding in the PEGylated nanoparticles, with the uptake of the photosensitizer being only about 5% of that measured when the free dye is incubated with the cells.

These results are important because they clearly indicate that the use of the PEGylated nanoparticles as a carrier for the photosensitizer should minimize unwanted uptake by healthy tissues and by consequence reduce the unwanted systemic toxicity of the therapy. On the other hand, this ability to escape cell capture makes conjugation with targeting agents necessary in order to trigger active uptake mechanisms and ensure that the photosensitizer is delivered to the target cells. We hence investigated the "in vitro" uptake of folate-, RGD- and Cetuximab-conjugated nanoparticles using cell lines over-expressing the targets recognized by each vehicle moieties. The results obtained are quite different with the three guided-nanosystems.

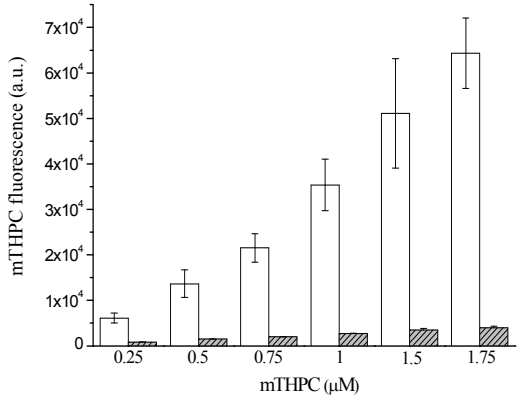

Figure 4. Flow cytometry measurements of mTHPC and derivative **4** uptake in A549 cells incubated for 24 h with increasing concentration of free mTHPC (white) or **4**-doped PEG-ORMOSIL nanoparticles (grey).

In the case of folate, KB cells overexpressing and A549 cells not expressing the folate receptor were used. The presence of the folate in the nanoparticles coating results in (see ESI): i) decreased uptake with respect to nanoparticles coated with only PEG; ii) no difference in the uptake of folate-nanoparticles between KB and A549 cells (not shown) and; iii) no inhibition of the uptake of folate-targeted nanoparticles in KB cells preincubated with 1 mM free folic acid to saturate the receptor and prevent the internalization of the nanoparticles through the receptor-driven specific endocytosis. Such behavior is not affected by the size of the nanoparticles or by the thickness of the PEG coating or the length of the PEG functioning as a linker for folate.

Different results were obtained with the RGD-targeted nanoparticles incubated with HUVEC cells overexpressing the integrin $\alpha_v\beta_3$ receptors for RGD. We evaluated the efficiency of the targeting agent on the same cell line by comparing the uptake of the RGD-targeted nanoparticles with that of identical particles (prepared from the same original batch) targeted with the RAD peptide, where the substitution of the central glycine with an alanine prevents the recognition by the integrins. Inspection of the results reported in Figure 5 provides evidence of higher uptake of the RGD-conjugated nanoparticles with respect to the RAD-conjugated ones. The uptake improves by increasing the amount of RGD peptides present in the nanoparticles coating layer form 15 to 30%, while uptake slightly decreases using smaller nanoparticles (40 nm diameter). The different behaviour

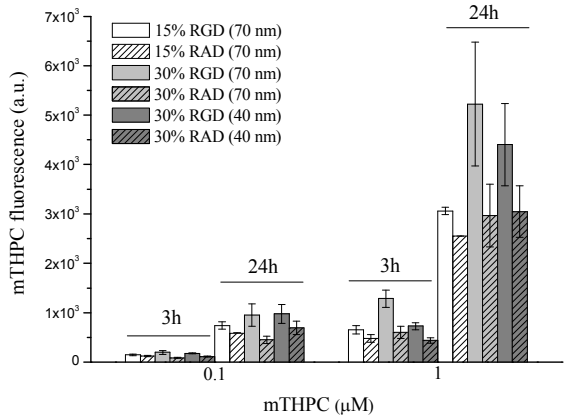

Figure 5. Flow cytometry measurements of mTHPC derivative **4** uptake in HUVEC cells incubated for 3 or 24 h with **4**-doped PEG-ORMOSIL nanoparticles of different size and conjugated with RGD and RAD peptides in different amounts.

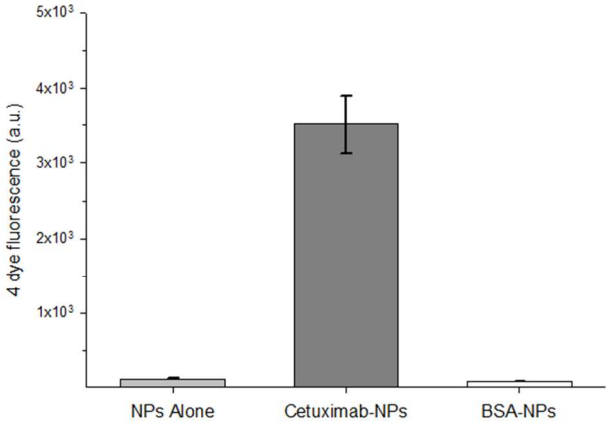

Figure 6. Differential uptake of **4**-doped PEG-ORMOSIL nanoparticles unconjugated (NPs alone), or conjugated with Cetuximab and BSA on A431 cells. Cells were incubated with nanoparticles at 1 μM concentration of dye 4 for 90 minutes at 37°C, nanoparticle uptake was analyzed by flow cytometry.

between the two small-molecule targeting agents is not unprecedented in PLGA nanoparticles and was attributed to poor surface exposure of the hydrophobic folate moiety.[28] Moreover, it has been recently reported that a dense PEG layer coating silica nanoparticles can effectively capture and incorporate organic dyes from water solution.[29] It can hence be expected that the long PEG3300 linker, bearing the targeting agent, folds allowing to the folate moiety to hide in the PEG layer. In support of this view, some of us recently found that only liposomes with a degree of PEGylation not higher than 8% the folate conjugation slightly improved the selectivity of mTHPC uptake in KB cells.[30] Furthermore, the decreasing uptake of folate ORMOSIL nanoparticles with the increasing of the folate percentage might indicate changes of the surface properties that make cell internalization less efficient. The zwitterionic RGD peptide is much more hydrophilic than folate and hence it is likely less attracted by the PEG pseudophase, therefore remaining available for the interaction with the cellular receptor.

Such a picture is confirmed by the results obtained with the **4**-doped nanoparticles conjugated with the antibody Cetuximab (Figure 6). Here the size of the targeting agent (i.e. the average size of an antibody is 15×8×4 nm[31]) is such that the interference of the PEG coating with its binding efficiency appear to be unlikely. In fact, internalization of targeted nanoparticles at 37°C, measured on the A431 cells overexpressing the EGF receptor, is impressive. The uptake of the conjugated nanoparticle is at least 20-fold greater than that of the unconjugated or BSA-conjugates (prepared as negative control systems). The specific uptake of Cetuximab-guided nanoparticles on A431 cells was confirmed by competition experiments performed by co-incubating cells, at 37°C, with increased concentrations of free Cetuximab (Figure 7). In fact the co-incubation of targeted nanoparticles with free Cetuximab reduces the nanoparticle uptake of about 93%, whereas no decrease of nanosystem uptake is observed for BSA-conjugated control particles in the same conditions (see ESI).

Further assays were performed to obtain more insight on the internalization mechanism. First the dependence of the uptake by the amounts of Cetuximab or BSA-conjugated nanoparticles added was investigated (see ESI) and demonstrated that the internalization mechanism of the antibody-guided nanovectors is saturable. In fact, the amount of taken-up nanoparticles does not increases linearly with the amount of nanoparticles added and appears to reach a plateau for nanoparticles concentrations of 320 μg/mL (corresponding to a dye concentration of 4 μM). Such behavior suggests that, once all the EGF receptors available on the surface of the cells are bound to antibodies conjugated with the nanoparticles, further increments of the nanoparticles concentrations do not result in increased uptake, as expected for a receptor mediated internalization mechanism. Indeed the BSA-conjugated nanoparticle uptake appears to follow a different trend with a linear concentration-dependent increase of the uptake in the interval studied.

The same picture emerged from time-dependant analysis performed using in this case three different cell lines (see ESI):

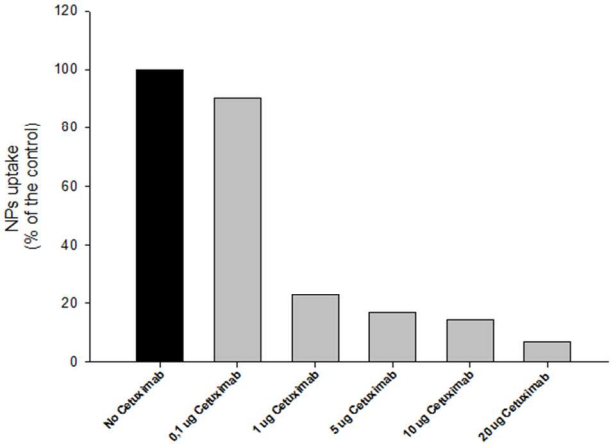

Figure 7. Displacement of the uptake of **4**-doped PEG-ORMOSIL nanoparticle conjugate with Cetuximab on A431 cells by free Cetuximab. Cells were incubated with nanoparticles at 0.25 μM concentration of dye **4** and increasing concentrations of free Cetuximab for 90 minutes at 37°C, nanoparticles uptake was analysed by FACS.

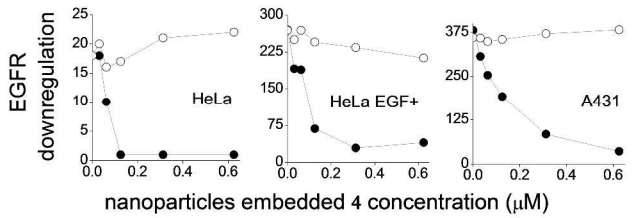

Figure 8. Nanoparticles induced down-regulation (measured as amount of cell bound FITC-labelled anti EGFR antibody) of EGF receptor in different cell lines. Cells were incubated in DMEM 10 % FCS with different concentrations of Cetuximab (●) or BSA (○) conjugated nanoparticles for two hours at 37°C; washed and analysed by FACS. Note the different signal intensities in the three cell lines, proportional to plasma membrane EGFR amounts.

normal HeLa cells, expressing basal amounts of plasma membrane located EGFR, a derived HeLa cell lines, permanently transfected to express higher levels of surface EGFR (4-5 folds the parental HeLa cell line) and the above mentioned A431 cells, expressing a high amount of EGFR (10-13 folds in the plasma membrane compared to HeLa cells). As expected, Cetuximab-conjugated nanoparticles uptake is not linear with incubation time and reaches a saturation level after about 2 hours with all the cell lines. Moreover, the amount of nanoparticles taken up at saturation is directly correlated with the extent of EGFR expression levels, with A431 and transfected HeLa internalizing upon prolonged incubation an amount of nanoparticles about 20- and 4-fold larger than normal HeLa. On the other hand, non-specific uptake of BSA-conjugated nanoparticles appears to occurs with a slower and cell line-independent kinetic that does not reach saturation values in the time span explored. As a consequence, maximum preferential uptake is observed for short incubation times.

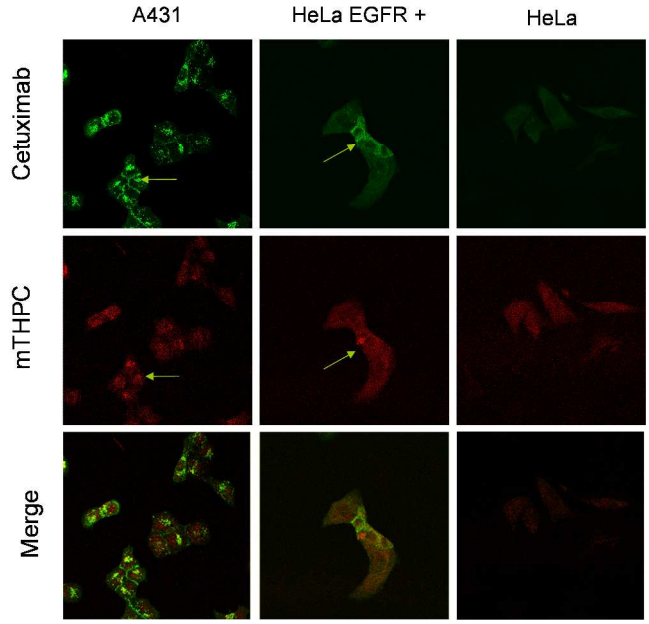

Figure 9. Colocalization of Cetuximab and dye **4** upon incubation of EGFR positive A431 cells, EGFR over-expressing HeLa and parental HeLa (having reduced EGFR levels) with Cetuximab conjugated **4**-doped ORMOSIL nanoparticle at 1 μM mTHPC concentration for two hours at 37°C. Green signal is Cetuximab distribution, red one is mTHPC. Arrows point the colocalisation of Cetuximab and mTHPC.

The specific interaction of the nanoparticles with EGFR, followed by internalisation of the resulting complex, was clearly documented by further experiments in which the amount of surface receptors was quantified by FACS after incubation with nanoparticles using a fluorescein-conjugated Cetuximab as a label (Figure 8). Indeed, Cetuximab-conjugated nanoparticles, but not BSA-conjugated ones, down regulate EGFRs in all cell types, suggesting, in agreement with confocal microscopy (see infra), that complexes between Cetuximab-nanoparticles and EGFRs, formed on the plasma membrane, are internalised in endosomes and this leads to a decrease of the amount of receptor on the cell surface. EGFR down regulation is complete at very low nanoparticles concentrations (50 μg/mL for A431 cells, corresponding to a **4** concentration of 0.62 μM). Confocal microscopy analysis experiments (Figure 9) enabled localisation of both nanoparticle-linked Cetuximab (by staining with a fluorescein labelled anti-human antibody) and of the nanoparticle-linked dye **4**. The experiment confirmed that the nanoparticles bind more effectively to cells overexpressing the EGFR, with localized emission of dye **4** suggesting endosomial localization, while the high degree of colocalization of Cetuximab and **4** indicates that the nanoparticles maintain their integrity upon internalization.

Taken together, all these experiments confirm an active uptake mechanism, where the targeted nanoparticles bind to the EGF receptors available on the cell surface and are internalized by endocytosis. On the other hand, untargeted nanoparticles are taken up by a slow and non saturable passive mechanism. Hence, optimal selectivity can be achieved for relatively low doses and incubation times.

Finally from the perspective of future "in vivo" evaluations, we investigated the serum stability of our protein conjugated-nanosystems. The nanoparticles functionality, assessed as binding and uptake capabilities on A431 cells, decreases of less than 20% when the incubation of Cetuximab-conjugated nanoparticles was performed in 100% of serum (i.e. 90 minutes at 37°C). The good serum stability was also confirmed when longer incubation times were applied (i.e. 32% of functionality was preserved after 16hrs of serum pre-treatment, data not shown).

PDT experiments

The phototoxicity of **4** delivered by nanoparticles was determined both in the case of RGD- and Cetuximab-conjugated nanoparticles. In the case of RGD nanoparticles, a significant reduction of the cell viability was found after irradiation of the cells incubated with the **4**-loaded nanoparticles, demonstrating the photokilling activity of the dye embedded in the nanoparticles. Disappointingly, the dose-response curve obtained by treatment of the HUVEC cells with RGD-conjugated nanoparticles was in any case perfectly superimposed (see SI) to that of RAD-conjugated nanoparticles. A possible explanation of such a behaviour is based on the findings of Allen and co-workers that suggest that RGD, but not RAD, partially protect the cells from PDT induced death by exerting an anti-oxidant and/or anti-apoptotic effect.[32]

Better results were obtained with the Cetuximab-conjugated nanoparticles (Figure 10), but only when prolonged (6 hours)

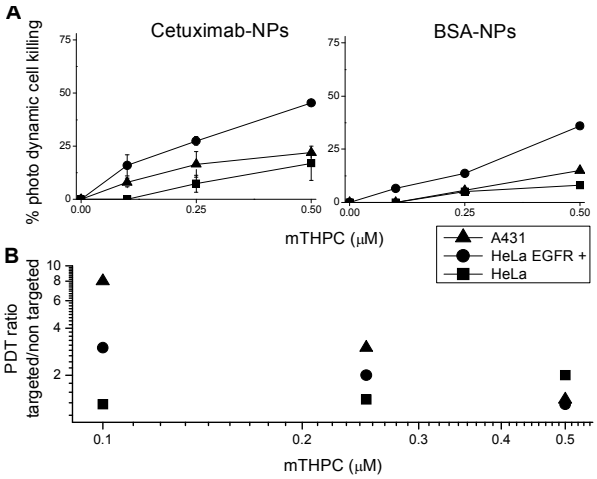

Figure 10. Photokilling efficiency of Cetuximab- and BSA-conjugated 4-loaded PEG-ORMOSIL nanoparticles upon incubation for 6 hours with different cell lines and light exposure. A) Amount of cell killed with respect to the control at increasing nanoparticle doses. B) Ratio of photokilling activity between targeted and control nanoparticle on the different cell lines as a function of the dose administered.

incubation times where applied. As revealed from figure 10A, absolute photokilling efficiency does not correlate with uptake in the different cell lines, likely as a result of a different ability of the cell line to resist to cytotoxicity of generated ROS. However, when the attention is focused on the difference between the activity of the targeted and untargeted nanoparticles with each cell line, it appears evident as the Cetuximab-conjugated nanoparticles are substantially more efficient in photokilling A431 cells (up to 8-fold) than the BSA-conjugated counterparts when delivered at doses well below the EGF receptors saturation level. This difference rapidly decreases when the nanoparticles dose is increased, possibly because the non-specific uptake of the untargeted particles becomes more relevant with respect to the receptor-mediated uptake at this prolonged incubation times, or when cells express a lower (HeLa-EGFR, 40% of EGFR with respect to A431) or negligible (HeLa) amount of EGF receptor.

Shorter incubation times at low doses led to negligible photokilling. As a matter of fact, when compared with free mTHPC delivered as standard formulation, Cetuximab-conjugated nanoparticles are still less efficient in producing photoxicity. The photochemical investigations reported in the previous paragraph exclude the possibility that such a result arises from a lower efficiency of singlet oxygen production by the nanoparticle-embedded photosensitizer. On the other hand, unfavourable localization of the nanoparticles inside the cells could result into a lower cytotoxic activity of the singlet oxygen produced. In fact, it is well-known that mTHPC mainly localises in the Golgi apparatus and the endoplasmic reticulum, while we have showed here that **4**-loaded Cetuximab-conjugated nanoparticles are found essentially in endosomal vesicles.

Conclusions

In summary, the results reported provide interesting insight on how to optimise the properties of VTES-ORMOSIL nanoparticles for biomedical applications, and in particular for targeted therapy. Being designed to operate in a very complex environment such as a living organism, such nanoparticles require a precise design which in turn needs detailed chemical and structural characterization. The first feature that emerges is the flexibility of the synthetic procedure, which enables the one-pot preparation of nanoparticles loaded with the active agent, PEGylated and either targeted or ready for post-targeting. However, realization of such a multifunctional entity requires taking into account all the possible interactions between the components. The organosilica matrix provides a low polarity environment that preserves the photochemical properties of the embedded photosensitizer while maintaining water accessibility, but excessive rigidity of the framework, as here in the case of tetrasilane derivative **5**, may result in an unanticipated perturbation to the photophysical properties in aqueous solution leading to a reduced singlet oxygen yield. Dense PEGylation minimizes toxicity and RES capture, but also uptake by cells. This enables higher selectivity with active targeting strategies, as we demonstrated using the Cetuximab targeting agent. On the other hand, the possibility of adverse interactions between the targeting molecules and the stealth-conferring layer to which they are grafted, as here in the case of folate, must be taken in to account and prevented.

Another important feature is the interaction with proteins, which is fundamental in determining the final fate of a nanoparticle following administration. The results reported herein suggest that not only we can prevent such interactions, as is well known, by coating the particles with PEG or other hydrophilic molecules, but also we can select the interacting proteins by finely tuning the surfaces properties, as here shown in the case of VTES and Stöber particles.

Finally, we explored the crucial point of selective targeting and the importance of the subcellular fate of the nanoparticles. The results we report on RGD and Cetuximab-conjugated nanoparticles clearly show that increased uptake arising from efficient targeting is not sufficient to ensure higher therapeutic efficiency. In particular data obtained with Cetuximab were very informative, since they clearly indicate that differential binding to tumor model cells of nanoparticles and hence of mTHPC loading may be achieved only at doses of ligand-linked nanoparticles that do not saturate the internalization mechanism. Once these specific sites are saturated, non-specific and non-saturable binding sites become more relevant upon increasing the applied nanoparticle concentrations. The resulting paradox is that *selective* photokilling was only achieved under conditions of *partial killing efficacy*. Moreover, subcellular localization may also play an important role in explaining the correlation between uptake and PDT efficacy, since the amount of photosensitizer internalized could not be a good parameter to evaluate the real amount of effective photosensitizer, i.e. the fraction localized at critical sites more susceptible to generated ROS.

These observations may lead to the development of new strategies to improve the intrinsic efficacy of the nanoparticles-carried photosensitizer inside the cell, a parameter that, in the end, appears to be the most critical and limiting to gain effective neoplastic cell disruption. The implementation of active release mechanisms or the addition of other chemical determinants to the nanoparticle coating layer capable of re-directing them to more sensitive intracellular sites/organelles, or helping their translocation to the cell cytoplasm, could provide solutions to this

problem. All this information provides a useful framework in the development of new nanosystems for tumor therapy.

Acknowledgements

Financial support for this research has been provided by European Union (FP7, grant 201031 NANOPHOTO, and FSE post-doc fellowship, DGR n. 1102, to F.S.), by the Italian Ministry of Research (FIRB 2011, RBAP114AMK RINAME) and by the University of Padova (PRAT CPDA110213), by Fondazione Cariverona (Verona Nanomedicine Initiative project), by AIRC 5×1000 and by Fondazione Cariverona/AIRC Progetto Regionale. The Varian 400 SS-NMR spectrometer used was acquired by the University of Padova thanks to funding from the Fondazione CARIPARO (Progetti di Eccellenza ''Nano-Mode'' 2010).

The authors thank Matteo Bachicchetto for performing some preliminary experiments and Biolitec research GmbH (Jena, Germany) for supplying Temoporfin (mTHPC).

Notes and references

[a] *Dipartimento di Scienze Chimiche, Università di Padova, via Marzolo 1, Padova, I-35131, Italy. Tel:+39 0498275666; Fax: +39 0498275239. E-mail: fabrizio.mancin@unipd.it*

[b] *Dipartimento di Biologia, Università di Padova, via U. Bassi 58/B, Padova, I-35131, Italy. Tel: +39 0498276335; Fax: +39 8276300. E-mail: elena.reddi@unipd.it*

[c] *Dipartimento di Scienze Biomediche e Centro di Ricerca Inter-dipartimentale per le Biotecnologie Innovative, Università di Padova, via U. Bassi 58/B, Padova, I-35131, Italy. Fax: +39 0498276301 Tel: +39 0498276159. E-mail: emanuele.papini@unipd.it*

[d] *University College London Medical School, National Medical Laser Centre, 67-73 Riding House St, London W1W7EJ, UK. E-mail: E-mail: a.macrobert@ucl.ac.uk*

[e] *Dipartimento di Patologia e Diagnostica, Università di Verona, Piazzale A Scuro 10 , Verona , I-37134, Italy. Fax: +39 045-8124256 Tel: +39 0458126455. E-mail: marco.colombatti@univr.it*

[‡] *These authors equally contributed to the work.*

† Electronic Supplementary Information (ESI) available: Experimental procedures and nanoparticles additional characterization. See DOI: 10.1039/b000000x/

1 (a) M. W. Ambrogio, C. R. Thomas, Y.-L. Zhao, J. I. Zink and J. F. Stoddartt, *Acc. Chem. Res.*, 2011, **44**, 903-913; (b) S.-H. Wu, Y. Hung and C.-Y. Mou, *Chem. Commun.*, 2011, **47**, 9972-9985; (c) P. Couleaud, V. Morosini, C. Frochot, S. Richeter, L. Raehm and J.-O. Durand, *Nanoscale*, 2010, **2**, 1083-1095; (d) J. L. Vivero-Escoto, I. I. Slowing, B. G. Trewyn and V. S. Y. Lin, *Small*, 2010, **6**, 1952-196; (e) W. J. M. Mulder, G. J. Strijkers, G. A. F. Van Tilborg, D. P. Cormode, Z. A. Fayad and K. Nicolay, *Acc. Chem. Res.*, 2009, **42**, 904-914; (f) Y. Piao, A. Burns, J. Kim, U. Wiesner and T. Hyeon, *Adv. Funct. Mater.*, 2008, **18**, 3745-3758.

2 *Colloidal Silica: Fundamentals and Applications;* H. E. Bergna and W. O. Roberts, eds.; CRC Press: Boca Raton, 2006.

3 (a) A. Burns, P. Sengupta, T. Zedayko, B. Baird and U. Wiesner, *Small*, 2006, **2**, 723-726; (b) A. Vanblaaderen and A. Vrij, *Langmuir*, 1992, **8**, 2921-2931.

4 B. G. Trewyn, I. I. Slowing, S. Giri, H.-T. Chen and V. S. Y. Lin, *Acc. Chem. Res.*, 2007, **40**, 846-853.

5 (a) J. Hu, M. Chen, X. Fang and L. Wu, *Chem. Soc. Rev.*, 2011, **40**, 5472-5491, (b) X. Du and J. He, *Nanoscale*, 2011, **3**, 3984-4002; (c) L. Bau, B. Bartova, M. Arduini and F. Mancin, *Chem. Commun.*, 2009, 7584-7586.

6 M. Arduini, F. Mancin, P. Tecilla and U. Tonellato, *Langmuir*, 2007, **23**, 8632-8636.

7 L. Bau, P. Tecilla and F. Mancin, *Nanoscale*, 2011, **3**, 121-133.

8 R. Ciriminna, M. Sciortino, G. Alonzo, A. de Schrijver and M. Pagliaro, *Chem. Rev.*, 2011, **111**, 765-789.

9 I. Roy, T. Y. Ohulchanskyy, H. E. Pudavar, E. J. Bergey, A. R. Oseroff, J. Morgan, T. J. Dougherty and P. N. Prasad, *J. Am. Chem. Soc.*, 2003, **125**, 7860-7865.

10 T. Y. Hulchanskyy, I. Roy, L. N. Goswami, Y. Chen, E. J. Bergey, R. K. Pandey, A. R. Oseroff and P. N. Prasad, *Nano Lett.*, 2007, **7**, 2835-2842.

11 S. Kim, T. Y. Ohulchanskyy, H. E. Pudavar, R. K. Pandey and P. N. Prasad, *J. Am. Chem. Soc.*, 2007, **129**, 2669-2675; see also: M. Gary-Bobo, Y. Mir, C. Rouxel, D. Brevet, I. Basile, M. Maynadier, O. Vaillant, O. Mongin, M. Blanchard-Desce, A. Morere, M. Garcia, J. O. Durand, L. Raehm, *Angew. Chem. Int.* Ed. 2011, **50**,11425-11429.

12 S. Kim, T. Y. Ohulchanskyy, D. Bharali, Y. Chen, R. K. Pandey and P. N. Prasad, *J. Phys. Chem. C*, 2009, **113**, 12641-12644.

13 S. Kim, H. E. Pudavar and P. N. Prasad, *Chem. Commun.*, 2006, 2071-2073.

14 W.-C. Law, K.-T. Yong, I. Roy, G. Xu, H. Ding, E. J. Bergey, H. Zeng and P. N. Prasad, *J. Phys. Chem. C*, 2008, **112**, 7972-7977.

15 (a) D. J. Bharali, I. Klejbor, E. K. Stachowiak, P. Dutta, I. Roy, N. Kaur, E. J. Bergey, P. N. Prasad and M. K. Stachowiak, *Proc. Natl. Acad. Sci. U. S. A.*, 2005, **102**, 11539-11544; (b) I. Roy, T. Y. Ohulchanskyy, D. J. Bharali, H. E. Pudavar, R. A. Mistretta, N. Kaur and P. N. Prasad, *Proc. Natl. Acad. Sci. U. S. A.*, 2005, **102**, 279-284.

16 R. Kumar, I. Roy, T. Y. Hulchanskyy, L. N. Goswami, A. C. Bonoiu, E. J. Bergey, K. M. Tramposch, A. Maitra and P. N. Prasad, *ACS Nano*, 2008, **2**, 449-456.

17 (a) A. Gupta, L. N. Goswami, M. Ethirajan, J. Missert, K. V. R. Rao, T. Ohulchanskyy, I. Roy, J. Morgan, P. N. Prasad and R. K. Pandey, *J. Porphyrins Phthalocyanines*, 2011, **15**, 401-411; (b) C. Compagnin, L. Bau, M. Mognato, L. Celotti, G. Miotto, M. Arduini, F. Moret, C. Fede, F. Selvestrel, I. M. Rio Echevarria, F. Mancin and E. Reddi, *Nanotechnology*, 2009, **20**, 345101.

18 a) I. M. Rio-Echevarria, F. Selvestrel, D. Segat, G. Guarino, R. Tavano, V. Causin, E. Reddi, E. Papini and F. Mancin, *J. Mater. Chem.*, 2010, **20**, 2780-2787; b) I. M. Rio-Echevarria , R. Tavano, V. Causin, E. Papini, F. Mancin and A. Moretto, *J. Am. Chem. Soc.* 2011, **133**, 8-11.

19 D. Segat, R. Tavano, M. Donini, F. Selvestrel, I. Rio-Echevarria, M. Rojnik, P. Kocbek, J. Kos, S. Iratni, D. Scheglmann, F. Mancin, S. Dusi and E. Papini, *Nanomedicine*, 2011, **6**, 1027-1046.

20 R. Tavano, D. Segat, E. Reddi, J. Kos, M. Rojnik, P. Kocbek, S. Iratni, D. Scheglmann, M. Colucci, I. M. Rio Echevarria, F. Selvestrel, F. Mancin and E. Papini, *Nanomedicine*, 2010, **5**, 881-896.

21 W. Stober, A. Fink and E. Bohn, *J. Colloid. Interface. Sci.*, 1968, **26**, 62-69.

22 (a) Z. Olejniczak, M. Leczka, K. Cholewa-Kowalska, K. Wojtach, M. Rokita and W. Mozgawa, *J. Mol. Struct.*, 2005, **744**, 465-471; (b) Y. J. Eo, D. J. Kim, B. S. Bae, K. C. Song, T. Y. Lee and S. W. Song, *J. Sol-Gel Sci. Technol.*, 1998, **13**, 409-413. (c) D. L. Ou and A. B. Seddon, *J. Non-Cryst. Solids*, 1997, **210**, 187-203.

23 A. Vanblaaderen and A. P. M. Kentgens, *J. Non-Cryst. Solids*, 1992, **149**, 161-178.

24 D. F. Moyano and V. M. Rotello, Langmuir, 2011, **27**, 10376-10385.

25 In contrast, a hydrophilic trianionic phorphyrin covalently embedded into mesoporous silica nanoparticles prepared by the Stöber procedure efficiently produce single oxygen with a quantum yield of 0.57 in ethanol, see: D. Brevet, M. Gary-Bobo, L. Raehm, S. Richeter, O. Hocine, K. Amro, B. Loock, P. Couleaud, C. Frochot, A. Morère, P. Maillard, M. Garcia and J.-O. Durand, *Chem. Commun.*, 2009, 1475-1477

26 a) Y. Ferrand, *Bioorg. Med. Chem. Lett.*, 2003, **13**, 833-835; b) M. Wacker, K. Chen, A. Preuss, K. Possemeyer, B. Roeder and K. Langer, *Int. J. Pharm.*, 2010, **393**, 253-262.

27 a) M. Ravikanth, and T. K. Chandrashekar, *J. Photochem. Photobiol. A: Chem.*, 1993, **74**, 181-187; b) B . Röder, M. Büchner, I. Rückmann and M. O. Senge, *Photochem. Photobiol. Sci.*, 2010, **9**, 1152-1158.

28 P. M. Valencia, M. H. Hanewich-Hollatz, W.Gao, F. Karima, R. Langer, R. Karnik, and O. C. Farokhzad, *Biomaterials,* 2011, **32**, 6226-6233.

29 a) D. Genovese, M. Montalti, L. Prodi, E. Rampazzo, N. Zaccheroni, O. Tosic, K. Altenhoner, F. May and J. Mattay, *Chem. Commun.*, 2011, **47**, 10975-10977; b) E. Rampazzo, S. Bonacchi, R. Juris, M. Montalti, D. Genovese, N. Zaccheroni, L. Prodi, D. C. Rambaldi, A. Zattoni and P. Reschiglian, *J. Phys. Chem. B*, **2010**, 114, 14605-14613.
30 F. Moret, D. Scheglmann and E. Reddi, *Photochem. Photobiol. Sci*. 2013, *in press*, DOI: 10.1039/c3pp25384h.
31 G. Amit, R. A. Mariuzza, S. E. Phillips, R. J. Poljak, *Science,* 1986, **233**, 747-753.
32 C. M. Allen, W.M. Sharman, C. La Madeleine, J. E. van Lier and J. M. Weber, *Photochem. Photobiol. Sci.*, 2002, **1**, 246-254.

GRAPHICAL ABSTRACT

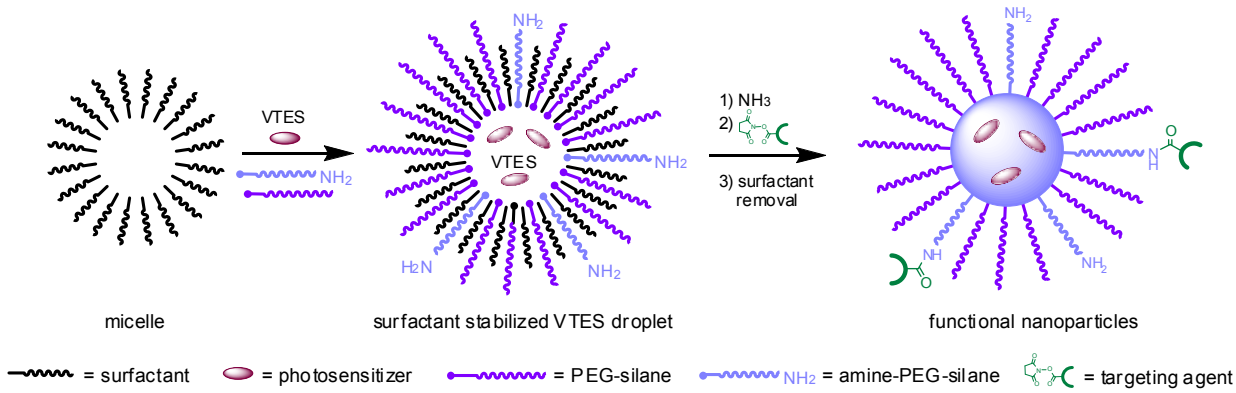

Highly flexible ORMOSIL nanoparticles can be PEGylated, doped with photoactive species, targeted for selective recognition of cancer cells.